Characterization of Electro-materials using ac Impedance Spectroscopy

DEREK C. SINCLAIR

Departament of Chemistry. University of Aberdeen, Meston Walk, Aberdeen, U. K. AB9 2UE

Caracterización de electromateriales mediante el empleo de espectroscopía de impedancia

Se discute y revisa la teoría básica de la espectroscopia de impedancia y se exponen varios ejemplos de electromateriales/dispositivos, donde las medidas de impedancia compleja dan una excelente información, que no puede ser obtenida por técnicas ac y dc convencionales. Se hace énfasis en las técnicas avanzadas de adquisición y elaboración de datos; por ejemplo la combinación de los diagramas de espectroscopia de impedancia con la espectroscopia del modulo eléctrico, para caracterizar electricamente materiales cerámicos inhomogeneos como los materiales basados en BaTiO3 que son resistencias con coeficiente de temperatura positivo. Se presenta un análisis eléctrico detallado de monocristales ferroeléctricos de LiTaO3 en función de la orientación cristalográfica. Los resultados demuestran la utilidad de la técnica de impedancia para visualizar procesos tan complejos como la inversión de dominios en materiales ferroeléctricos. Se discute también el uso de estas técnicas in-situ para monotorizar variaciones en las capas intercaras en las intercaras electrodo-electrolito en las baterías de litio de estado sólido.

Palabras clave: Electromateriales, Espectroscopia de impedancia, Espectroscopía de módulo eléctrico.

The basic theory of ac impedance spectroscopy is reviewed and then several examples of electro-materials/devices are discussed where ac impedance measurements have provided information which is not readily available from dc or conventional fixed frequency ac measurements. Emphasis is given to advanced data handling techniques, such as combined impedance and electric modulus spectroscopic plots for characterising electrically inhomogeneous ceramics such as positive temperature coefficient of resistance BaTiO$_3$ ceramics. A detailed electrical analysis of ferroelectric LiTaO$_3$ single crystals as a function of crystallographic orientation is presented. These results demonstrate the usefulness of the technique in monitoring complex processes such as domain reversal in ferroelectric materials. The use of in-situ ac impedance measurements to monitor variations in interfacial layers at electrode-electrolyte interfaces in solid state lithium batteries is also discussed.

Key words: Electromaterials, Impedance Spectroscopy Electric-Modulus Spectroscopy.

1. INTRODUCTION

Electrical applications of solid-state materials cover the complete spectrum from electrical insulators to superconductors. The desired properties are many and varied but can be sub-divided into four main categories:

(i) intra-granular or "bulk" properties, e.g. high levels of ionic conductivity, such as Na$^+$ ion conduction in beta-alumina ceramics, used as an Na$^+$ ion conducting membrane in Na/S batteries [1].

(ii) intergranular or "grain boundary" properties, e.g. resistive grain boundary components and conducting cores, such as doped-SrTiO$_3$ internal barrier layer capacitors [2],

(iii) a combination of both inter- and intra-granular properties, e.g. positive temperature coefficient of resistance (ptcr) devices, such as donor-doped BaTiO$_3$, which depend on resistive grain boundary components and ferroelectric semiconducting grains [3], or

(iv) surface properties, e.g. gas sensors [4], such as SnO$_2$.

Invariably these high-technology ceramics require specialised knowledge regarding the structural, compositional, ceramic processing and electrical behaviour of the material(s) in question. Consequently there are many aspects of electro-ceramics which need to be studied and combined in order to obtain a complete characterisation of the material under investigation.

By far the largest application of ferroelectric materials is the development of various types of capacitors [5]. All these devices rely on the material being an electrical insulator with a large bulk permittivity value. In recent years, ferroelectric materials have found increasing application in other diverse areas of electro-ceramics and composite materials, namely as ptcr devices, pyro- and piezo-electric sensors and electro-optic devices. As further applications of these polar solids emerge, characterisation of their behaviour, by existing and new techniques becomes imperative.

The two main techniques employed in the characterisation of electro-ceramics are microscopy and electrical measurements.

Scanning, SEM, and transmission microscopy, TEM, are commonly employed to characterise the microstructure. Advanced techniques, such as dark and bright field imaging have been developed in recent years to detect thin layers, 10 nm, of amorphous

second phase material in the grain boundary regions of electroce-ramics [6], such as ZnO varistors. Combining such techniques with EDAX, energy dispersive analysis of X-rays, allows the composition of these regions, or the distribution of a dopant between the bulk and grain boundary regions to be determined.

Decoration techniques, such as integral, ICL, and spectral, SCL, cathodoluminescence have been developed to make grain boun-dary potential barriers visible in materials such as ptcr BaTiO$_3$ [7,8]. These techniques, which "bridge the gap" between micros-tructural and electrical measurements, depend on the number of electrons in the conduction band. Resistive regions appear dark whereas conductive regions are bright. Thus, resistive regions in a ceramic may be identified by combining CL techniques and elec-tron microscopy. These techniques are becoming increasingly popular in characterising the microstructure of many electro-cera-mics.

DC electrical measurements, two or four terminal, are the most commonly employed method of establishing electrical characteris-tics of electro-ceramics, although they are not the most convenient method of obtaining inter- and intra-granular resistance values. Recently, several groups [9,10] have developed techniques invol-ving micro-electrodes which permit direct measurements of the resistances associated with individual grains and grain boundaries. Such techniques are extremely useful but are very difficult to imple-ment experimentally.

A much more convenient method in which to separate surface, grain boundary and bulk components of a material is to employ ac impedance techniques over a wide frequency range, 10^{-2} to 10^7 Hz. Although this technique is commonly employed to esta-blish the bulk resistance of solid electrolytes [11], applications of this technique to grain boundary or interfacial layer dominated electro-materials/devices , such as ZnO varistors, ptcr devices and solid state batteries, etc., or to ferroelectric materials have been limited.

In the present paper, the basic theory of ac impedance spectros-copy is reviewed and several applications of the technique discus-sed in order to demonstrate how ac impedance spectroscopy can, under certain circumstances, yield information about electro-mate-rials/devices which is not readily available from dc or conventio-nal, fixed frequency ac measurements.

2. AC THEORY

AC impedance methods have been widely used to characterise electrical materials [12,13] and electrode-aqueous electrolyte sys-tems [14]. The most common method employed to study the ac res-ponse of a test system, i.e. an electrode-material arrangement, is by the direct measurement of the impedance in the frequency domain. The impedance of any system is defined as $Z = V_0/I_0$ and usually contains both resistive (R) and reactive (L and/or C) components, both of which must be determined. By applying a single frequency voltage $v = V_0.\sin(\omega t)$, where ω represents the angular frequency $2\pi f$, across the test system, the phase shift and amplitude of the resultant current $i = I_0.\sin(\omega t + \phi)$ can be determined. Unless the test system behaves as an ideal resistor there will be a phase diffe-rence, ϕ between the applied voltage and the resultant flowing current. The phase shift is related to the reactive component of the system. In general, both the magnitude (resistive) and phase shift (reactive) of the impedance of a sample is frequency dependent.

Impedance is a vector quantity which can be defined as a com-plex number, whose magnitude and direction can be expressed by real, Z' and imaginary, Z'' components.

$Z^* = Z'$ (resistive) $-jZ''$ (reactive)

where $j = \sqrt{-1}$. Three other complex formalisms can be measured or derived from the complex impedance:

(i) The complex admittance, Y^*, or A^*, is defined as the inverse of the complex impedance, Z^*:

$Y^* = (Z^*)^{-1} = Y' + Y''$.

The real component, Y', is more commonly known as the con-ductivity, σ.

(ii) The complex electric modulus, M^*, is related to the complex impedance, Z*, through the relation:

$M^* = j\omega C_0 Z^* = M' + M''$

where $C_0 = \varepsilon_0 A/l$ is the vacuum capacitance of the empty mea-suring cell with electrode area, A, and separation, l. The permitti-vity of free space $\varepsilon_0 = 8.854 \times 10^{-14}$ Fcm^{-1}.

(iii) The complex permittivity, ε^*, can be defined as the inverse of the complex electric modulus, M*:

$\varepsilon^* = (M^*)^{-1} = Y^*(j\omega C_0)^{-1} = \varepsilon' + \varepsilon''$.

Although the four basic formalisms are interrelated they can be subdivided into two sets, i.e. (Z*, M*) and (Y*, ε^*) from the equa-tions above. The main effect of the transformation within each set is to exchange the real and imaginary components on multiplica-tion by ω, as shown above. Thus, all four formalisms are valuable, because of their different dependence on, and weighting with, fre-quency. It is this feature of versatility, where the various polarisa-tion and charge transfer processes which occur in a test system, over the measured frequency range, are highlighted by different for-malisms, which gives ac techniques such power in the studies of electrical properties of matter.

There are various forms in which the data may be plotted:

(i) a locus of points in the complex plane, i.e. imaginary against the real component,

(ii) a spectroscopic plot, i.e. the real and imaginary components as a function of log (f),

(iii) a combined spectroscopic plot, i.e. the real or imaginary components of the different formalisms as a function of log (f),

(iv) a three dimensional plot, with log (f) perpendicular to the complex plane.

Despite this versatility, the majority of workers present the ac res-ponse of dielectric/ferroelectric and conducting materials only in the ε^* and Z* planes, respectively.

The different regions of a test system are normally characterised by a resistance and capacitance, usually placed in parallel. The characteristic relaxation time or time constant, τ of each parallel RC element is given by the product of R and C, i.e. $\tau = RC$. In the frequency domain, RC elements are separable due to the rela-tionship $\omega_{max}.RC = 1$ which holds at the frequency of the maxi-mum loss, ω_{max}, in the impedance spectrum. From the impedance spectrum, it is usually possible to identify different RC elements, based on the capacitance values, and assign them to the appro-priate regions of the test system. The values of the individual R and C components may then be quantified.

In this analysis, different physical features in the test system are represented by layers of varying thickness, as in Maxwell's model of the layered dielectric [15] (fig. 1). This model assumes that the permittivity of the various regions, namely, any surface layer adja-cent to the electrodes, the grain boundary regions and the grain interiors, all have the same value.

The equation for a parallel plate capacitor is defined as:

$C = \varepsilon' C_0$

where ε' is the permittivity of the material placed between the plates and C_0 is the vacuum capacitance. The capacitance values associated with these three regions discussed above differ only in the value of l. Differences in capacitance are therefore, a direct
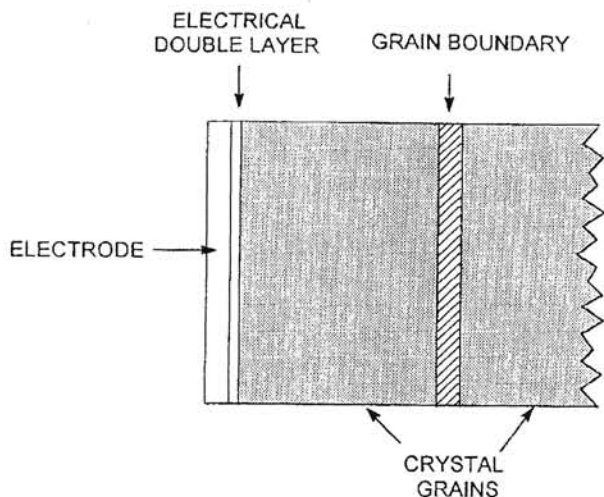
56

Boletín de la Sociedad Española de Cerámica y Vidrio. Vol. 34 Núm. 2 Marzo-Abril 1994

ELECTRICAL
DOUBLE LAYER   GRAIN BOUNDARY

ELECTRODE

CRYSTAL
GRAINS

Figure 1. *Physical representation of a sample/electrode arrangement in terms of Maxwell's layered dielectric model.*

result of the relative thickness of each region. The grain boundary regions are 10^{-2} - 10^{-4} and the electrode interface $< 10^{-7}$, of the cell length. Typical capacitance values and their possible interpretation for a unit cell are listed in table I. Thus, small capacitance values e.g. 10^{-12} Fcm^{-1} are associated with large volume fractions, i.e. bulk material, whereas larger capacitances, e.g. 10^{-9} Fcm^{-1} to 10^{-6} Fcm^{-1} are associated with progressively smaller volume fractions or with the bulk response of ferroelectric materials with large values of permittivity. These "order of magnitude" values enable a correlation between the observed electrical properties and the various regions within a test system.

TABLE I. CAPACITANCE VALUES AND THEIR POSSIBLE INTERPRETATION[16]

Capacitance/ Fcm^{-1}	Phenomenon Responsible
10^{-12}	bulk
10^{-11}	minor, second phase
10^{-11} - 10^{-8}	grain boundary
10^{-10} - 10^{-9}	bulk ferroelectric near T_c (Curie Temperature)
10^{-9} - 10^{-7}	surface layer
10^{-7} - 10^{-5}	sample-electrode interface
10^{-4}	electrochemical reactions

The central problem associated with ac measurements arises over the interpretation of the data collected. The ac response for a test system defines only the relationship between the applied voltage and the current through the test system, as a function of frequency. The physical nature of the test system i.e. single crystal, polycrystalline, blocking or non-blocking electrodes, etc, and its electrical properties i.e. ionic, electronic or mixed conductor, ferroelectric, etc, must be considered. Plausible equivalent circuits, i.e. some network containing ideal resistive and reactive components may then be suggested which can represent these properties of the system and model the collected data.

There are materials whose electrical behaviour is such that ideal resistive and capacitive circuit elements are inadequate to describe the ac response. This has led to the introduction of distributed impedance elements [17,18], e.g. CPE, the constant phase element,

which "mix" "ideal" resistive and reactive elements to model the observed response. The degree of success in any ac analysis depends on how well the experimental data fit that predicted by an appropriate equivalent circuit.

An equivalent circuit that contains three or more elements may be rearranged in various combinations but still yield the same overall ac response. This leads to the notion that there is no unique equivalent circuit for a particular test system. The values of the elements for the circuits have to be different in order to yield the same overall response. Thus, the problem arises as to which equivalent circuit should be employed for the analysis and interpretation of the electrical behaviour of a test system. Usually, the equivalent circuit is chosen based on the following:

(i) intuition as to what kind of impedances are expected to be present in the test system and whether they are connected in series or parallel,

(ii) examination of the experimental data to decide whether the response is consistent with the proposed circuit,

(iii) inspection of the R and C values that are obtained in order to check that they are realistic and their temperature dependence, if any, is reasonable.

The equivalent circuit shown in figure 2 is widely used to represent bulk and grain boundary phenomena in polycrystalline materials. It is desired to separate each of the parallel RC elements and measure their component R and C values. This is best achieved using a combination of the impedance and electric modulus formalisms since each parallel RC element gives rise to a semicircle in the complex plane (Z'' vs Z'; M'' vs M') or a Debye peak in the spectroscopic plots of the imaginary component (Z'', M'' vs log f). This is seen from the equation for the impedance of the circuit:

$$Z^* = (1/R_1 + j\omega C_1)^{-1} + (1/R_2 + j\omega C_2)^{-1}$$
$$Z^* = Z' - jZ''$$

where

$$Z' = R_1/\{1 + (\omega R_1 C_1)^2\} + R_2/\{1 + (\omega R_2 C_2)^2\}$$

and

$$Z'' = R_1[\omega R_1 C_1/\{1 + (\omega R_1 C_1)^2\}] + R_2[\omega R_2 C_2/\{1 + (\omega R_2 C_2)^2\}]$$

The corresponding equations for M' and M'' are obtained by substituting into the equation $M^* = j\omega C_0 Z^*$. These are

$$M' = (C_0/C_1).\{(\omega R_1 C_1)^2/ (1 + (\omega R_1 C_1)^2)\}+ (C_0/C_2).\{(\omega R_2 C_2)^2/ (1 + (\omega R_2 C_2)^2)\}$$

and

$$M'' = (C_0/C_1).[\omega R_1 C_1/\{1 + (\omega R_1 C_1)^2\}] + (C_0/C_2).[\omega R_2 C_2/ \{1 + (\omega R_2 C_2)^2\}]$$

Note that the terms in square brackets for the Z'' and M'' components is a mathematical representation of a Debye peak.

The response of this circuit in the two complex plane plots is shown in figure 3. For convenience and to illustrate the relative weightings that impedance and modulus plots apply to data, the values of R_1 and R_2 are chosen to differ by a factor of 100, but the capacitances are chosen to be equal. In the complex impedance
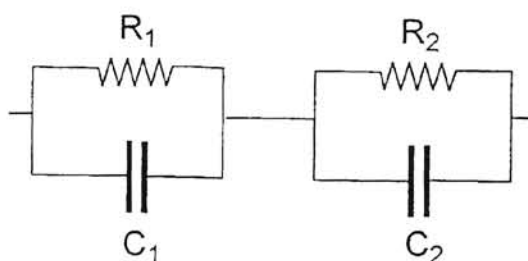
R_1 R_2

C_1 C_2

Figure 2. An equivalent circuit commonly used to represent the electrical properties of a polycrystalline material. The subscripts 1 and 2 refer to electrically distinct regions within the material, e.g. bulk and grain boundary components.
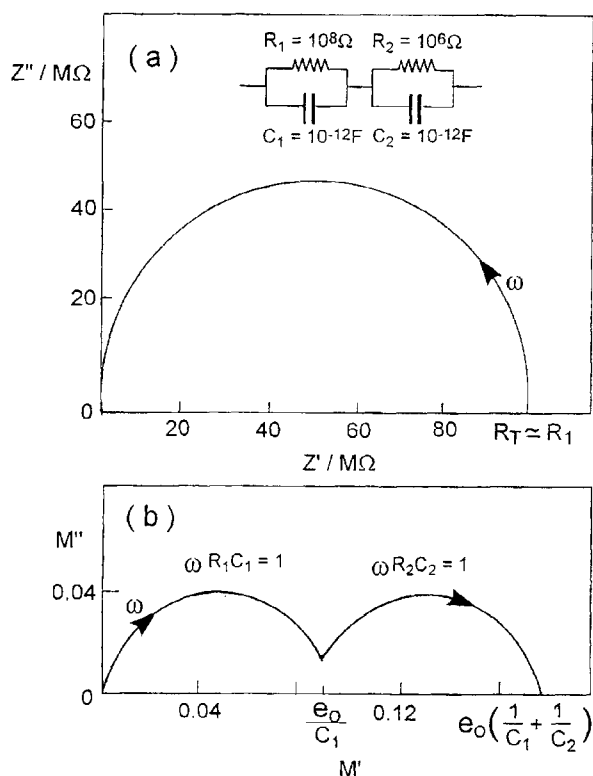
Figure 3. *Complex impedance (a) and electric modulus (b) plane plots for the circuit shown.*
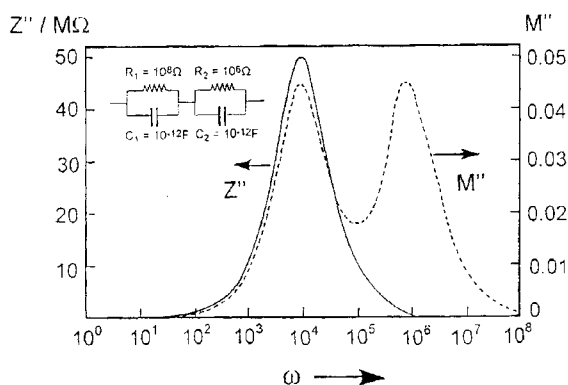

Figure 4. *Impedance, Z'', and electric modulus, M'', spectroscopic plots against frequency, $\omega = 2\pi f$ for the circuit shown.*

plane, a single semicircle is seen since the impedance response is dominated totally by the parallel RC circuit with the larger resistance, R_1. In the modulus plane, two semicircles, of equal size, are seen because the modulus response is dominated by the RC element with the smaller parallel capacitance, and in this case, the capacitances are equal.

The spectroscopic plots show a similar effect, figure 4, with a single peak in Z'' but two peaks in M''. An advantage of the combined Z'', M'' plot such as this is that the M'', Z'' peaks for a particular RC element should be coincident on the frequency scale, as indeed they are for the lower frequency of the two peaks. A rapid assessment can therefore be made from a visual inspection of such a combined plot. This comparison is not so easy to do for the complex plane plots since, whereas the Z^* plane plot terminates at the origin at the high frequency limit, the M^* plane commences at the origin at the low frequency limit.

The frequencies of peak maxima in Z'' and M'' spectroscopic

plots are given by the respective relaxation time constants for the given parallel RC element. The RC product for each peak is a fundamental parameter as also is the value of ω_{max}. This is because the RC product is usually independent of the geometry of the region responsible for the RC element.

In the particular example shown in figures 3 and 4, the modulus plots show up both parallel RC elements, whereas the impedance plots only show the more resistive element. On varying the magnitudes of R and C components, however, different situations may arise. For instance, if one of the capacitances is much larger than the other, its associated peak and semicircle will effectively disappear from the modulus plots. The key point in determining whether RC elements are detected depends on which plot is used and the relative magnitudes of the capacitances. Thus modulus plots give emphasis to those elements with the smallest capacitances, whereas impedance plots highlight those with the largest resistances.

The response in the Z^* plane for a single parallel RC element ideally takes the form of a semicircular arc which passes through the origin and gives a low frequency intercept on the real axis corresponding to the resistance, R of the element, figure 5. In practice, semicircles associated with bulk relaxation processes in the Z^* plots of many conducting materials and in the ε^* plots of dielectric (insulating) materials, are found to be non-ideal. Depressed semicircles are obtained whose centres are displaced below the real axis; they occur for both single crystal and polycrystalline materials. There are two main reasons for such non-ideal behaviour:

(i) the presence of a distribution in relaxation times within the bulk response, and

(ii) distortion by other relaxations , e.g. grain boundary relaxations, whose time constants are within two orders of magnitude of that of the bulk.

These resolution problems can limit somewhat the use of ac techniques in characterisation of individual electrical and electrochemical processes. Curve fitting programs for two overlapping arcs and more generally, complex non-linear least squares (CNLS) analysis can be employed [19, 20] in an attempt to overcome such problems.

In general, metal electrodes are applied to ionic and electronic conducting materials. For ionic conducting materials there are two extreme types of metal contacts, blocking and non-blocking. Gold electrodes are commonly employed and are blocking. For Li^+ conductors, the gold/Li^+ conductor interface has been modelled by a voltage independent parallel plate capacitor [21, 22]. The model consists of an electronically charged metal surface in direct contact with an equal but oppositely charged Li^+ layer residing within the first atomic layer of the Li^+ conducting material.

Several assumptions are made in this model; namely, no specific adsorption or ion migration to or from the interfaces occur and that the outer surfaces of the material are smooth and contain no voids. Figure 5 (a) summarises the equivalent circuit and ideal ac response in the Z^* plane for a single crystal ionic conductor with blocking electrodes. The semicircular arc, with intercepts on the real axis at 0 and R, represents the response of a parallel R_1C_1 bulk element. At low frequencies the Z^* plane response is dominated by the blocking nature of the electrode interface, where

$-Z'' = 1/\omega C$. This response is illustrated by a vertical locus of points, often referred to as an electrode "spike", in which $-Z''$ decreases with increasing ω. This data can be modelled by an equivalent circuit whereby the bulk parallel RC element is connected in series with an ideal capacitor which represents the blocking nature of the electrode interface.

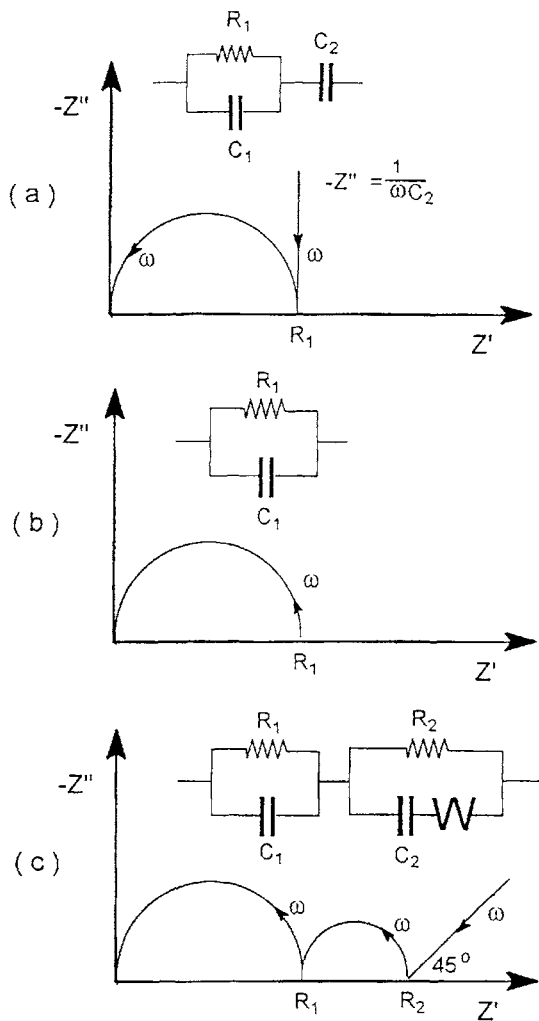In practice, however, electrode contacts are jagged and contain

Figure 5. *Complex impedance plots and equivalent circuits proposed for materials exhibiting bulk; (a) ionic conduction with blocking electrodes, (b) electronic conduction with ohmic contacts and (c) infinite, Warburg-type ionic diffusion with an associated charge transfer element, R_2C_2.*

electrically open and closed circuits as well as a host of adsorbed and foreign species, all of which influence the local electric field. In general, the interface impedance is partly resistive and partly capacitive. This results in a low frequency electrode spike in the Z^* plane whose angle is less than $\pi/2$. To model such systems often requires the use of CPE's or transmission lines to account for any frequency dispersion of the electrode response [23-25]. In the present paper such complexities are ignored: instead, blocking electrode interfaces are represented as double layer capacitances in series with the sample impedance.

Non-blocking or reversible electrodes allow conduction of both electrons and mobile ions, at very high discharge rates, across the electrode/sample interface. Since there is no charge build-up or polarisation, such as occurs with blocking electrodes, $C_{dl} = 0$ and the Z^* plane response does not contain a low frequency spike, figure 5 (b). For gold electrode systems this behaviour would normally identify electronic species as the predominate charge carriers of a sample.

In other cases, the rates of discharge of mobile ions at the electrodes may be slow enough to be measurable; such electrodes are said to be partially blocking. In this case, finite or infinite diffusion of the mobile charge carriers occurs into the electrode material.

This results in an inclined low frequency spike in the Z^* plane plot of angle ca. $\pi/6$ to $\pi/2$. In addition to an inclined spike, a low frequency semicircle is commonly observed in the Z^* plane plot, figure 5 (c). This response, with an associated capacitance in the order of $10^{-6} Fcm^{-1}$, permits a resistance value (R_2 in figure 5 (c)) for the charge transfer mechanism of the mobile ions between the electrode/sample interface to be calculated. Partial blocking behaviour of gold electrodes also normally identifies ionic conduction within a sample.

An inclined spike of angle $\pi/4$, where $|Z'| = |Z''|$ involves infinite diffusion of the mobile species into the electrode material. This type of response is commonly referred to as Warburg-type behaviour, and is represented by the symbol W in equivalent circuit analyses, figure 5 (c).

The various combinations of electrode behaviour likely to occur for ionic conducting materials with both negatively and positively charged conducting species, their equivalent circuits and ac response in the Z^* plane have been extensively reviewed in the literature [22, 25] and are outside the scope of the present paper.

For electronic materials such as insulators, semiconductors and metals there are also two types of electrode behaviour, referred to as ohmic and non-ohmic contacts.

Ohmic contacts produce a minimum potential drop at the electrode interface when current is flowing through the material. Ohmic contacts are achieved by careful matching of the contact potentials, or work functions [26] of the material and metal electrode. Failure to match the contact potentials results in the creation of potential barrier at the interface. This results in a measurable potential drop at the electrode interface and is referred to as a contact resistance. Such electrodes are called non-ohmic contacts and would give rise to a low frequency semicircle in the Z^* plane plot.

In summary, the low frequency response in the Z^* plane can usually provide information on the nature of the predominant charge carriers responsible for the observed electrical conduction and on the physical processes which occur at the sample/electrode interface.

3. APPLICATIONS OF AC IMPEDANCE SPECTROSCOPY

In this section three applications of ac impedance spectroscopy are discussed.

(I) Solid-State Lithium Batteries

AC Impedance techniques provide one possible means of monitoring the cell performance of solid state batteries, e.g. Li [anode] / (PEO).LiCF$_3$SO$_3$ [polymer electrolyte] / V$_6$O$_{13}$ [cathode] and for yielding information on the chemical reactions and interfacial effects that occur during cell assembly and operation. Such techniques are commonly used to monitor polymer electrolyte conductivity and the formation of passivation layers at the anode/electrolyte and/or cathode/electrolyte interfaces [27-29].

An effect in these cells that has not been explained satisfactorily concerns their open circuit voltage (OCV) behaviour. Immediately after assembly and heating to their normal operating temperatures, e.g. 120°C, cells with polyethlene oxide electrolytes, e.g. PEO.LiCF$_3$SO$_3$ have reproducibly high OCV values, e.g. 3.65V at 120°C for cells containing V$_6$O$_{13}$ - based cathodes. On standing, however, the OCV quickly falls before levelling out to a steady value, e.g. 3.2V for V$_6$O$_{13}$. In a previous study we [30] were involved in using ac impedance spectroscopy to monitor the OCV stabilisation period.

(a) Li/PEO. LiCF$_3$SO$_3$ / cathode
120°C, OCV = 3.52V

(b) Equilibration of cell : Li/PEO, LiCF$_3$SO$_3$ / cathode at 103°C

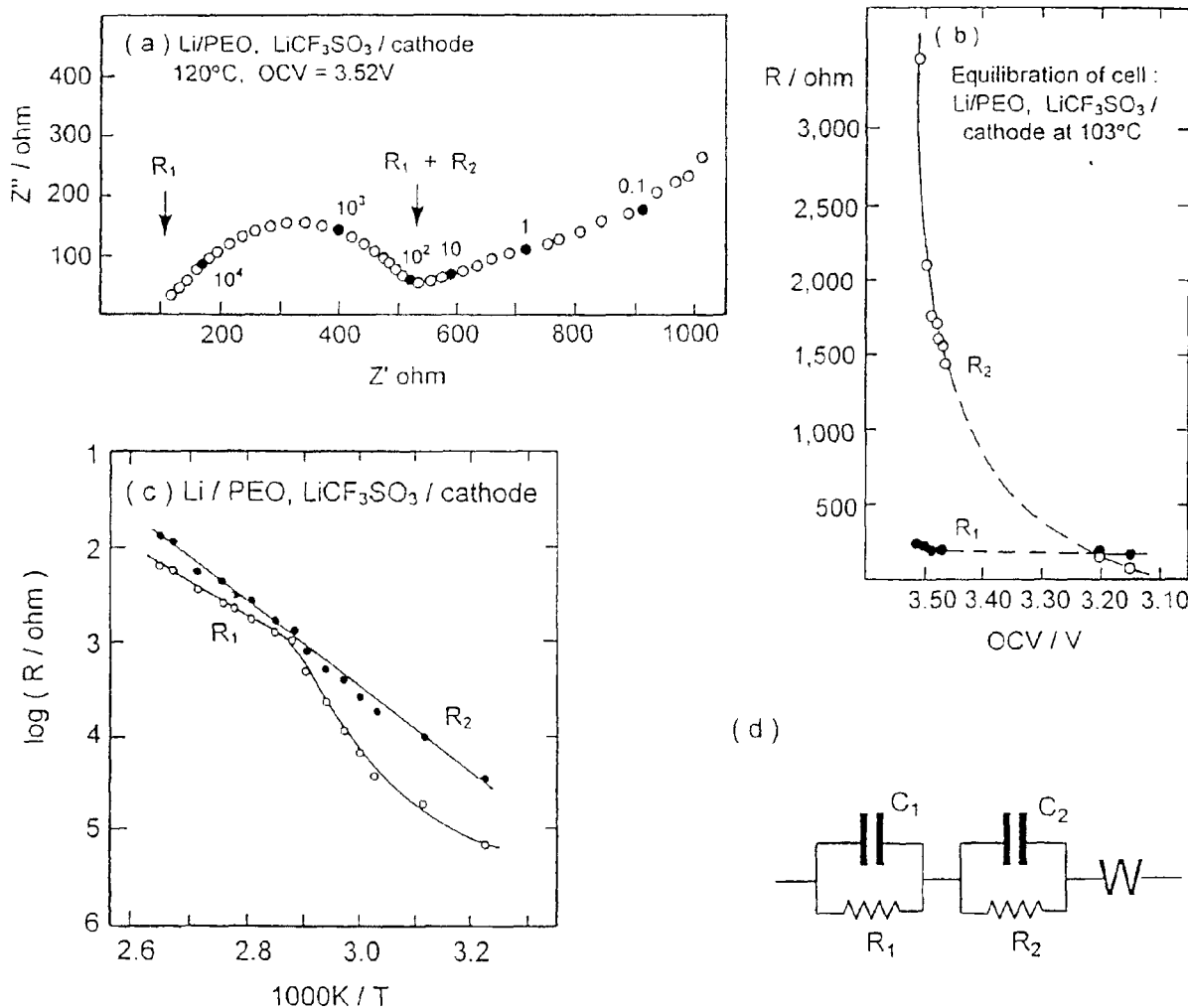**(c)** Li / PEO, LiCF$_3$SO$_3$ / cathode

(d)

Figure 6. (a) Complex impedance plane plot at 120°C for a freshly prepared cell. (b) Resistances R$_1$ and R$_2$ against OCV during the OCV stabilisation and (c) their variation with temperature. (d) The equivalent circuit used to model the ac impedance data.

The complex impedance spectra had a similar form throughout the equilibration period to that obtained initially, figure 6 (a). This comprised a single semicircle with a low angle spike at lower frequencies. The high frequency end of the semicircle clearly did not pass through the origin and gave a non-zero intercept, R$_1$. From the low frequency intercept on the real, Z' axis, a second resistance, R$_2$ could also be obtained, as shown.

During the period of OCV stabilisation, the resistance R$_2$ decreased markedly, by between 1 and 2 orders of magnitude, as shown in figure 6 (b), but R$_1$ showed little, if any, variation. The capacitance C$_2$ was also essentially unchanged throughout, with a value of 310±80nF.

In order to gain further insight into the origins of the two resistances R$_1$ and R$_2$, ac impedance measurements were made over the temperature range ambient to 120°C. A Li/(PEO).LiCF$_3$SO$_3$/V$_6$O$_{13}$ cell was left at 120°C for two days and then cooled slowly to room temperature over a period of 24h. The ac measurements were then made on the reheating cycle.

Results are given in figure 6 (c) in the form of log conductance versus reciprocal absolute temperature (no corrections were made for the cell constants). The resistance R$_1$ showed marked non-linear behaviour, with a change in slope at about 70°C, characteristic of PEO electrolytes. The R$_2$ data, by contrast, show essentially linear temperature dependence with no discontinuity.

The impedance data obtained below 50°C confirmed that R$_1$

was the bulk resistance of the electrolyte. An additional high frequency semicircle was also seen between the origin and the intercept R$_1$ in the impedance plots, not shown. This had an associated capacitance value consistent with the bulk capacitance of thin layer cells.

Symmetric anode and cathode cells, e.g. Li/PEO.LiCF$_3$SO$_3$/Li were prepared and their ac impedance recorded at different temperatures over the range 25 to 120°C. Only the symmetric anode cells showed evidence for the semicircular arc at intermediate frequencies, characterised by the R$_2$ C$_2$ element.

The ac impedance results on cells with different electrode-electrolyte combinations enables identification of certain features of the cells. The impedance data may be analysed in terms of the ideal equivalent circuit shown in figure 6 (d). The resistance R$_1$ represents the electrolyte resistance and is shunted by the cell geometric capacitance, C$_1$. Given the geometry of the cells, a value of C$_1$ in the range 30 - 300pF is reasonable. Arrhenius plots of the [R$_1$]$^{-1}$ values were of a similar form and, by comparison with literature reports, R$_1$ is consistent with the resistance of the polymeric electrolyte.

The parallel R$_2$C$_2$ element of figure 6 (d) was evident only in the impedance data for cells containing at least one lithium electrode. The presence of this element is therefore interpreted in terms of the Li/electrolyte interface. The magnitude of the capacitance C$_2$, in the range 30 - 400nF, suggests a thin layer extending over the range
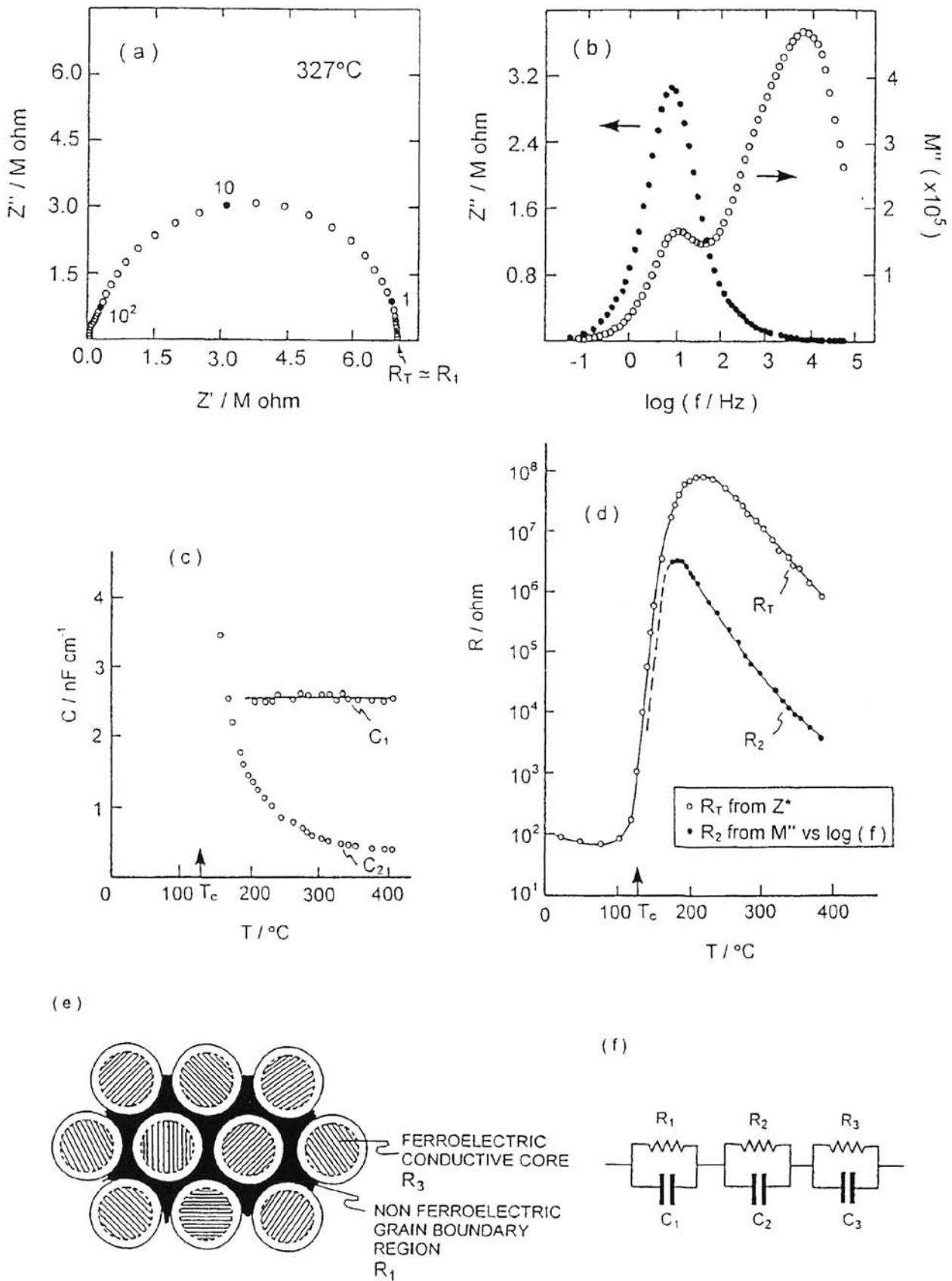
60

Figure 7. Impedance data for a ptcr BaTiO$_3$ ceramic at 327°C. The same data are used in (a) and (b) but are presented in different ways. Resistive and capacitance data as a function of temperature are shown in (c) and (d) and a schematic model and equivalent circuit of polycrystalline ptcr BaTiO$_3$ are shown in (e) and (f), respectively.

100 - 1000Å. This value of C_2 was relatively independent of both temperature and time. This would indicate, for such a model, that the layer thickness remains essentially constant. The observed variations of this R_2C_2 element are associated directly with the presence of a high initial open circuit voltage and its subsequent decline. Since it is known that $PEO.LiCF_3SO_3$ electrolytes decompose at voltages greater than 3.4 - 3.5V versus lithium at 120°C it is possible that the initial OCV decay is associated with a local decomposition of the electrolyte.

The Warburg resistance, figure 6 (d), is evidenced in the complex impedance plots by a low frequency spike, inclined ideally at 45°. The origin of the Warburg lies in the cathode material or at the electrolyte/cathode interface where significant intercalation of Li^+ in the V_6O_{13} -based cathode is expected.

Results such as these demonstrate the usefulness of ac impedance measurements in obtaining information regarding interfacial phenomena at both the anode and cathode interfaces with the polymer electrolyte. Such measurements are non destructive and can be used to monitor electrical phenomena in situ.

(II) Ptcr BaTiO₃ Ceramics.

The positive temperature coefficient of resistance, ptcr, effect is a well documented [31-34] but poorly understood phenomenon in which the electrical resistivity of certain materials undergoes a dramatic increase, often by several orders of magnitude, with increasing temperature. In donor-doped, semiconducting barium titanate, the ptcr effect occurs as the temperature is raised through the ferroelectric Curie-point, 120°C and in which the resistivity typically increases from ~100 Ωcm to ~100 MΩcm over an interval of about 100°C. The effect is fully reversible with temperature cycling and leads to applications in thermal fuses and current overload protection devices.

The origins of the ptcr effect are not well-understood. It is usually regarded as being associated with acceptor traps at the grain boundaries, e.g. adsorbed oxygen [35, 36], metal vacancies [37] and/or segregated additives/impurities i.e. manganese [38]. Various theories have been proposed to explain the effect, e.g. the Heywang model [39-40] whereby Schottky barriers are developed at the grain boundaries due to the acceptor traps, however many doubts remain [41-43].

In polycrystalline ceramic materials which exhibit modest levels of electronic conductivity, ac impedance techniques provide a powerful method for probing electrical inhomogeneities associated with crystal interiors, grain boundaries and surfaces. This is particularly the case when the results of different methods of data analysis are compared since often, one method alone, such as the use of complex impedance plane plots may give information that is incomplete or misleading. Recently we have shown that by use of combined impedance and modulus spectroscopy to analyse ac impedance data, it is possible to characterise both grain boundary and bulk phenomena in ptcr barium titanate ceramics [44-46]. This has lead us to develop a core-shell model to characterise these electrically inhomogeneous ceramics [47].

A typical complex impedance plane plot for a grain boundary dominated ptcr BaTiO₃ ceramic sample is shown in figure 7 (a). The spectrum consists essentially of a single semi-circular arc (capacitance $C_1 = 3$ nFcm⁻¹) associated with the resistive grain boundary component, such that the dc resistance of the sample, R_T approximates to R_1 at low frequencies, figure 7 (a). Given that impedance plane plots are dominated by the most resistive regions within a sample such plots are insensitive to the more conductive regions within the sample and therefore cannot be used as a method to probe such regions in ptcr BaTiO₃ ceramics.

A method of data processing which has been found to be very sensitive to probe the electrically inhomogeneous nature of these ceramics has been combined spectroscopic plots of the imaginary components of impedance, Z'' and electric modulus, M''.

As described in the previous section such plots place different weighting on, and highlight different features of the collected data. Z'' spectra are dominated by the most resistive element of the sample whereas M'' spectra are inversely proportional to capacitance and are more sensitive to the "bulk" or grain response of the sample, table 1.

Plots such as that shown in figure 7 (b) have provided information which has not previously been obtained from traditional Z^* plane plots of such materials [48, 49]. The Z'' spectra are dominated by the more resistive grain boundary component, R_1 and thus show only a single peak in the Z'' spectra, corresponding to the semicircle in figure 7 (a). In striking contrast to the single peaks in the Z'' plots, M'' plots based on the same raw data, show much more complexity with two (fig. 7 b), or in some cases three [46], overlapping peaks. Furthermore, M'' plots as a function of temperature show a marked variation in shape.

The smaller, lower-frequency peak which is coincident with the Z'' peak, fig 7 (b), stays at about the same size, indicating that its capacitance value is constant. The higher-frequency M'' peak increases in size with temperature, indicating that its capacitance value is decreasing. The associated capacitance values and temperature dependence of the two M'' peaks is shown in figure 7 (c); C_1 is essentially independent of temperature, whereas C_2 rises increasingly rapidly as the temperature decreases towards the Curie point. A Curie-Weiss plot for C_2, not shown, confirmed that C_2 was associated with a ferroelectric region of the sample above the Curie point and represents the polarisation of the residual domains which are present in the paraelectric region.

In order to determine the magnitudes of the two resistances, a combination of impedance and modulus plots is used. The value of the larger of the two resistances, R_1, is given directly from the complex impedance plane plots since, effectively, $R_{dc} = R_T = R_1$. The value of R_2 cannot be obtained from the impedance plots, but may be estimated from the ω_{max} value of the high-frequency M'' peak using the equation $\omega_{max} R_2C_2 = 1$, after its capacitance value has been determined($M''_{max} = C_0/C_2$). This resistance value for R_2 is plotted in figure 7 (d) and also exhibits a ptcr effect. Such an effect has not been previously discovered by use of dc or Z^* plane plots from ac measurements.

Detailed analysis of ac impedance data of such ptcr BaTiO₃ ceramics has led us to propose [47] the core-shell type model shown in figure 7 (e). In this model both R_1 (grain boundary) and R_2 (shell of individual grains) show ptcr effects, whereas R_3 (core of grains) remains semiconducting as the temperature is raised through the Curie point. The predominant acceptor states of the grain boundary and outer grain regions are thought to be adsorbed oxygen and metal vacancies (Ba and/or Ti), respectively. The capacitance associated with the grain boundaries, C_1, is independent of temperature and non-ferroelectric whereas the capacitance of the shell-type regions of the grains, C_2, has been shown to be ferroelectric. Due to the low resistivity of the core region, < 20 Ωcm, nothing is currently known about C_3 or its temperature dependence. The equivalent circuit used to model the ac response of the ptcr BaTiO₃ ceramics is shown in figure 7 (f) and comprises of a series array of parallel RC elements: each parallel RC element represents an electrical region of the sample, such as the grain boundaries or the crystal interiors.

Results such as these demonstrate how alternative formalisms of data presentations can yield additional information that is not easily
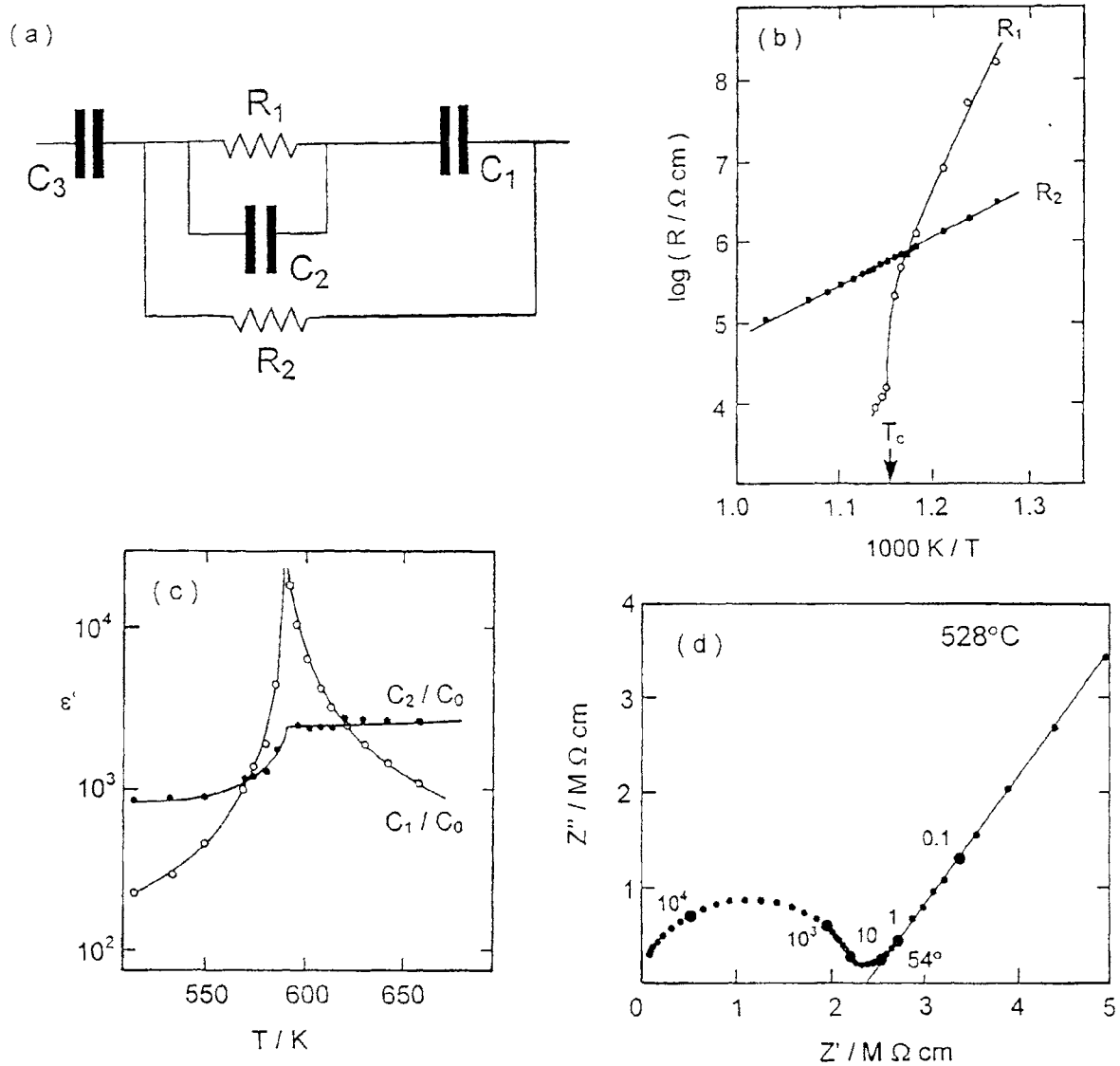
62

Boletín de la Sociedad Española de Cerámica y Vidrio. Vol. 34 Núm. 2 Marzo-Abril 1994

Figure 8. *Impedance data for single crystal $LiTaO_3$ with the applied voltage parallel to the polar c axis. The equivalent circuit, resistive and capacitive data and a complex impedance plane plot at 528°C for this orientation are shown in (a) to (d), respectively.*

accessible from the complex impedance plane alone and thus lead to a more complete characterisation of electrically inhomogeneous electro-ceramics such as ptcr $BaTiO_3$ ceramics.

(III) Single Crystal $LiTaO_3$

$LiTaO_3$ is a ferroelectric material and a modest conductor of lithium ions/electrons at high temperatures which finds numerous applications associated with its non-linear optical and pyroelectric properties. Studies on single crystals have the advantage that grain boundary phenomena should be absent and a more detailed analysis of the bulk properties may be made. ac Impedance measurements on single crystals of $LiTaO_3$ above and below the Curie temperature, ca 590°C, with the polar **c** axis orientated both parallel and perpendicular to the electric field, has allowed a detailed breakdown of the electrical properties for the different crystallographic orientations [50].

In the ferroelectric orientation i.e. applied electric field parallel to the polar **c** axis, the most useful methods of data analysis for R and C values was by complex admittance plane plots, Y*, and spectroscopic plots of the real component of permittivity, ε', respecti-

vely. The equivalent circuit and temperature dependence of the component R and C values are shown in figures 8 (a), (b) and (c) respectively. In this ferroelectric orientation, at temperatures below the Curie point the ac response of the sample indicates the presence of five components:

C_1, corresponds to the charge polarisation associated with the ferroelectric domains. It passes through a sharp maximum at Tc, figure 8 (c), and shows very good Curie-Weiss behaviour, extrapolating to the Curie temperature. Domain reversal is easiest in the region of the Curie point, as evidenced by the maximum in C_1 around 590°C. Well below the Curie temperature the value of C_1 is low since the domains are essentially fixed in their orientation and cannot be reversed at the small applied voltages, i.e. 100mV used in the impedance measurements. Above the Curie temperature, C_1 decreases as the domains break up into smaller clusters thus reducing the net polarisation.

R_1, in series with the ferroelectric capacitance C_1, figure 8 (a). This resistance is associated with the re-orientation of the ferroelectric domains and has a marked temperature dependence. Well below the Curie temperature the activation energy associated with complete domain reversal within the applied field is large and the-
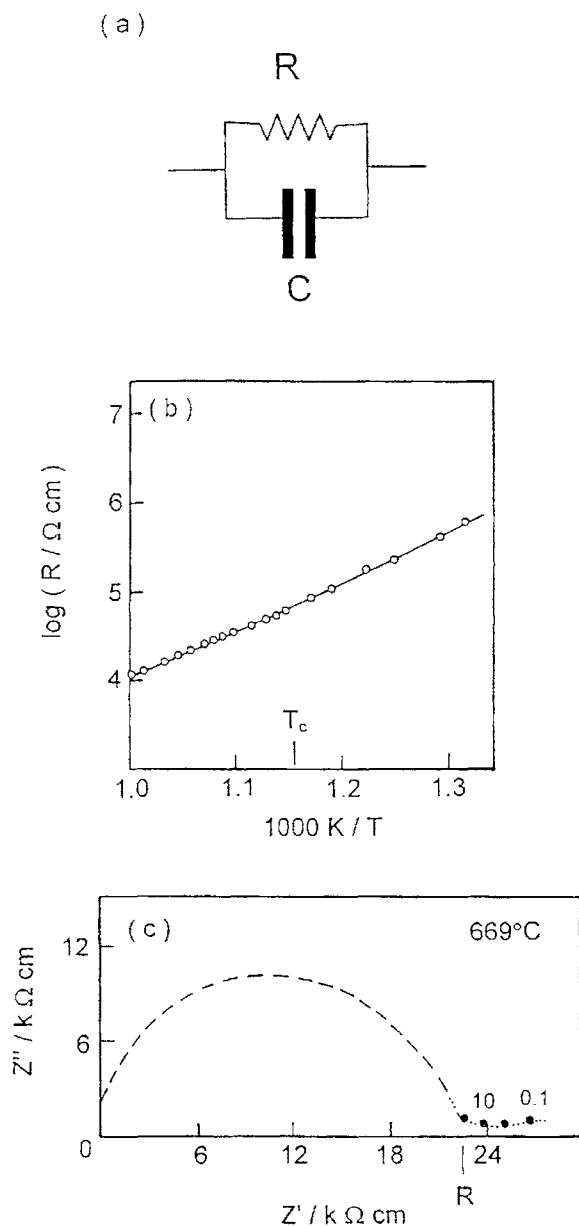
(a)

R

C

(b)

$\log (R / \Omega \, cm)$

T_c

1.0   1.1   1.2   1.3

1000 K / T

(c)   669°C

$Z'' / k \Omega \, cm$

12

6

0   6   12   18 | 24

$Z' / k \Omega \, cm$ R

Figure 9. *Impedance data for single crystal LiTaO3 with the applied voltage perpendicular to the polar c axis. The equivalent circuit, resistive data and a complex impedance plane plot at 669°C for this orientation are shown in (a) to (c), respectively.*

refore the associated resistance is large. As the Curie temperature is approached, switching of the ferroelectric domains in the applied field occurs more easily and the associated resistance R_1 decreases rapidly, with pronounced curvature, figure 8 (b) and the associated capacitance, C_1 increases, figure 8 (c). The small residual resistance above the Curie temperature can be attributed to the existence of local regions or clusters of ferroelectric polarisation.

C_2, in parallel with resistance R_1 represents the intrinsic lattice polarisation of the sample. Capacitance C_2 is not ferroelectric but it is very large and increases markedly on passing through the Curie temperature, figure 8 (c). This capacitance provides a measure of the small, individual atomic displacements of the Li and Ta ions within their distorted octahedral environments. The smooth increase in C_2 as the Curie temperature is approached can be related to the strong second-order character of the ferroelectric to paraelectric

transition. The polarisation of the individual dipoles starts to occur at temperatures well below the Curie temperature and is essentially optimised at the Curie temperature.

R_2, is in parallel with the other three elements and represents the leakage resistance of the crystal which is caused by the long range migration of Li^+ ions in this crystallographic orientation. It gives a linear resistance plot with an activation energy of 1.27eV, figure 8 (b).

C_3, is in series with the other four elements of the equivalent circuit, figure 8 (a) and represents the blocking double-layer capacitance associated with the crystal-electrode interface since the gold electrodes are blocking transport of the Li^+ ions. The magnitude of the capacitance was estimated from the low frequency spike in the complex impedance plane plots, figure 8 (d), using the equation Z'' = $1/\omega C$ and had a typical value of 2µF. The angle of the electrode spike is less than the ideal 90° due to the gold electrodes being only partially blocking towards Li^+ at such elevated temperatures.

In the non-ferroelectric orientation the impedance response is very simple and can be modelled by a single parallel RC element, figure 9 (a). There was no evidence of the resistance, R_1 and capacitance, C_1 attributed to the ferroelectric domains. Instead the material is a poor electronic conductor with a small, temperature-independent bulk capacitance.

Resistance values were obtained from the low frequency intercept of the semi-circular arc in the complex impedance plane plots. An Arrhenius plot of the data shows a slight change in slope at the Curie temperature with linear regions to either side, figure 9 (b). The low frequency region of the complex impedance plane plots did not show the existence of any characteristic electrode spike; instead a residual tail is observed, figure 9 (c). The absence of an electrode-spike indicates that the material is an electronic conductor in the non-ferroelectric orientation.

These results on LiTaO3 indicate the potential of ac impedance techniques for probing the electrical properties of ferroelectric crystals and demonstrate that ferroelectric domain reorientation can be characterised by macroscopic resistance and capacitance values. Such detailed characterisation of domain behaviour is much sought after but, as yet cannot be obtained from commonly-used fixed frequency or dc measurements.

4. SUMMARY

The basic theory, versatility and usefulness of ac impedance spectroscopy in characterising electro-materials and solid state devices has been reviewed. In these materials/devices, impedance spectroscopy has permitted detailed electrical characterisation of thin, interfacial layers between electrodes and electrolytes in solid state batteries and between grain and grain boundary regions in ptcr BaTiO3 ceramics. The usefulness of the technique in studying intrinsic properties of ferroelectric materials, such as electrical conduction and ferroelectric domain reversal is demonstrated by an in-depth study of single crystal LiTaO3 in different crystallographic orientations.

Data analysis for a given material/device normally requires more than one complex formalism to be studied and frequently, spectroscopic plots of either the real or imaginary components of a complex formalism have to be used in conjunction with complex plane plots. The results for LiTaO3 and ptcr BaTiO3 represent major advancements in characterisation over previous analyses which employed only dc or conventional fixed frequency and/or complex impedance plane plots of ac measurements. ◆

64

Boletín de la Sociedad Española de Cerámica y Vidrio. Vol. 34 Núm. 2 Marzo-Abril 1994

REFERENCES

1. D.P.Almond, A.R.West and R.J.Grant, Temperature Dependence of the ac Conductivity of Na-Beta-Alumina, Solid State Comms., **44** 1377 (1982) .

2. H.D.Park and D.A.Payne, Characterisation of Internal Boundary Layer Capacitors, Advances in Ceramics, **1**, 242, Ed. L.M.Levinson, The American Ceramic Society Inc.,Columbus, Ohio (USA) 1981..

3. B.M.Kulwicki, PTC Materials Technology, 1955-1980, Advances in Ceramics, **1**, 147, Ed. L.M.Levinson, The American Ceramic Society Inc.,Columbus, Ohio (USA) 1981..

4. P.T.Moseley and B.C.Tofield, "Solid State Gas Sensors." , 225, Adam Hilger, 1987.

5. A.J.Moulson and J.M.Herbert, "Electroceramics.", 189, Chapman and Hall, 1990,.

6. D.R.Clarke, The Microstructural Localisation of the Intergrannular Metal-Oxide Phase in a Zinc Oxide Varistor, J. Appl. Phys., **49** 2407 (1978).

7. H.Ihrig and M.Klerk, Visualisation of the Grain Boundary Potential Barriers of PTC-type $BaTiO_3$ Ceramics by Cathodoluminescence in an Electron-Probe-Micro-Analyser, Appl. Phys. Letts., **35** 307 (1980).

8. G.Koschel and E.Kubalek, Grain-Boundary Characteristics and their Influence on the Electrical Resistance of Barium Titanate Ceramics, J. Amer. Ceram. Soc., **68** 582 (1985).

9. D.Dimos, P.Chaudhari, J.Mannhart and F.K.LeGoues, Orientation Dependence of Grain-Boundary Critical Currents in $YBa_2Cu_3O_{7-x}$ Bicrystals, Phys. Rev. Letts., **61** 219 (1988).

10. H.Sumino, O.Sakurai, K.Shinozaki, M.Kato and N.Mizutani, A New Instruement to Measure the Electrical Properties in Very Narrow Regions in Ceramics, J. Mater. Sci. Letts., **10** 1026 (1991).

11. P.Wood, D.C.Sinclair and F.P.Glasser, Electrical Characterisation of Bismuth Orthovanadate Using ac Impedance Spectroscopy, Solid State Ionics, **66** 151 (1993).

12. K.S.Cole and R.H.Cole, Dispersion and Absorption in Dielectrics I. Alternating Current Characteristics, J. Chem. Phys., **9** 341 (1941).

13. J.E.Bauerle, Study of Solid Electrolyte Polarisation by a Complex Admittance Method, J. Phys. Chem. Solids, **30** 2657 (1969).

14. J.H.Sluyters and J.J.C.Oomen, The Impedance of Galvanic Cells. II. Experimental Evidence, Rec. Trav. Chim., **79** 1100 (1960).

15. L.Page and N.J.Adams, "Principles of Electricity" 2nd ed^n., Van Nostrand, 64 1949.

16. J.T.S.Irvine, D.C.Sinclair and A.R.West, Electroceramics: Characterisation by ac Impedance Spectroscopy, Adv. Mater., **2** 132 (1990).

17. A.K.Jonscher, "Dielectric Relaxations in Solids.", Chelsea Dielectric Press, 1983.

18. P.G.Bruce and A.R.West, The ac Conductivity of Polycrystalline LISICON $Li_{2+x}Zn_{1-x}GeO_4$ and a Model for Intergrannular Constriction, J. Electrochem. Soc., **130** 662 (1983).

19. J.R.Macdonald and J.A.Garber, Analysis of Impedance and Admittance Data for Solids and Liquids, J. Electrochem. Soc., **124** 1022 (1977).

20. J.R.Macdonald, "Impedance Spectroscopy", 180, John Wiley, 1987.

21. R.D.Armstrong, The Metal-Solid Electrolyte Interface, J. Electroanal. Chem., **52** (413 (1974).

22. R.D.Armstrong, Specalist Periodical Reports in Electrochemistry, **7** 157 (1980).

23. R. deLevie, The Influence of Surface Roughness of Solid Electrolytes on Electrochemical Measurements, Electrochim. Acta., **10** 113 (1965).

24. S.H.Liu, Fractal Mode for the ac Response of a Rough Interface, Phys. Rev.Letts., **55** 529 (1985).

25. M.Kleifz and J.Dupuy, "Electrode Processes in Solid State Ionics.", 149 Reidel Pub. Co., 1976

26. S.N.Sze, "Semiconductor Devices, Physics and Technology.", John Wiley, 1985.

27. N.C.Chaklanabish and H.S.Maiti, Discharge Characteristics and Interface Impedance of a $Li/1MLiClO_4(PC)/V_2O_5$ Cell, J. Power Sources, **16** 97 (1985).

28. J.Thevenin, Passivating Films on Li Electrodes - an Approach by means of Electrode Impedance Spectroscopy, J. Power Sources, **14** 45 (1985).

29. D.Fauteux, Formation of a Passivating Film at the Lithium-PEO-$LiCF_3SO_3$ Interface, Solid State Ionics, **17** 133 (1985).

30. C.C.Hunter, D.C.Sinclair, A.Hooper and A.R.West, ac Impedance Studies of the Lithium/Polymer Electrolyte Interface in Solid State Batteries, J. Power Sources, **24** 157 (1988).

31. O.Saburi, Properties of Semi Conducting Barium Titanates, J. Phys. Soc. Jpn., **14** 1159 (1959).

32. R.Wernicke, The Kinetics of Equilibrium Restoration in Barium Titanate Ceramics, Philips Res. Rep., **31** 526 (1976).

33. T.R.N.Kutty and P.Murugaraj, Electron-Paramagnetic-Resonance Study on the Role of Mn in Enhancing the PTC of $BaTiO_3$, Mat. Letts., **3** 195 (1985).

34. M.Kuwabara, Effect of Microstructure on the PTCR Effect in Semiconducting Barium Titanate Ceramics, J. Amer. Ceram. Soc., **64** 639 (1981) .

35. G.H.Jonker, Halogen Treatment of Barium Titanate Semiconductors, Mat. Res. Bull., **2** 401 (1967).

36. G.V.Lewis and C.R.A.Catlow, PTCR Effect in $BaTiO_3$, J. Amer. Ceram. Soc., **68** 555 (1985).

37. J.Daniels, K.K.Hardtl, D.Hennings and R.Wernicke, Defect Chemistry and Electrical Conductivity of Doped Barium Titanate, Philips Res. Rep., **31** 487 (1976).

38. T.R.N.Kutty, P.Murugaraj and N.S.Gajbhiye, EPR Evidence for Activation of Trap Centres in PTCR $BaTiO_3$ Ceramics, Mat. Res. Bull., **20** 565 (1985).

39. W.Heywang, Semiconducting $BaTiO_3$, J. Mater. Sci., **6** 1214 (1971)

40. G.H.Jonker, Some Aspects of Semi-Conducxting Barium Titanate, Solid State Electron., **7** 895 (1964).

41. H.Nemoto and I.Oda, Direct Examination of PTC Action of Single Grain Boundaries in Semi Conducting $BaTiO_3$ Ceramics, J. Amer. Ceram. Soc., **63** 398 (1980).

42. T.R.N.Kutty, Behaviour of Acceptor States in Semiconducting $BaTiO_3$ and $SrTiO_3$, Proc. Indian Acad. Sci., **96** 581 (1986) .

43. P.Gerthsen and B.Hoffmann, Current-Voltage Characteristics and Capacitance of Single Grain Boundaries in Semi-Conducting $BaTiO_3$, Solid State Electron., **16** 617 (1973).

44. D.C.Sinclair and A.R.West, Bulk PTCR Effect on Doped $BaTiO_3$, J. Mater. Sci. Letts., **7** 823 (1988).

45. D.C.Sinclair and A.R.West, Impedance and Modulus Spectroscopy of Semiconducting Barium Titanate Showing Positive Temperature Coefficient of Resistance, J. Appl. Phys., **66** 3850 (1989).

46. D.C.Sinclair and A.R.West, Variation with Processing Conditions of Bulk and Grain Boundary PTCR Phenomena in Doped $BaTiO_3$, "Surfaces and Interfaces of Ceramic Materials.", 535, Kluwer Acad. Pub., 1989.

47. D.C.Sinclair and A.R.West, Effect of Atmosphere on the PTCR Properties of $BaTiO_3$ Ceamics, J. Mater. Sci., **29** 6061 (1994).

48. R.N.Basu and H.S.Maiti, PTC Behaviour of Semiconducting $BaTiO_3$ Ceramics, Trans. Indian Ceram. Soc., **45** 140 (1986).

49. T.Y.Tseng and S.H.Wang, ac Electrical Properties of High-Curie-Point Barium-Lead PTCR Ceramics, Mater. Letts., **9** 164 (1990).

50. D.C.Sinclair and A.R.West, Electrical Properties of $LiTaO_3$ Single Crystal, Phys. Rev., **B39** 13486 (1989).

In Memoriam

JOSE RIVAS SANCHEZ

Falleció el día 17 de enero de 1995, a los 82 años de edad. Nacido en Oviedo, gran parte de su vida y actividades, transcurrieron entre Lugones y su ciudad natal.

Desde su juventud, participó activamente en la industria cerámica -Refractarios- donde llegó a alcanzar, los más altos puestos de mando y responsabilidad; primero en MERSA y después en DIDIER, S.A. hasta su jubilación.

En una larga etapa, década de los 40, hasta principio de los 90, desarrolló una intensa actividad, en defensa de los intereses de los fabricantes de productos refractarios. En una primera etapa, presidió el grupo de Refractarios, dentro del organigrama del Sindicato Vertical de Cerámica y Vidrio, y más tarde estuvo al frente de la Asociación Nacional de Fabricantes de Productos Refractarios (ANFRE) hasta que, al finalizar 1992, cesó a petición propia, siendo nombrado Presidente de Honor, de dicha Sociedad.

Miembro fundador de la Sociedad Española de Cerámica y Vidrio, tuvo una participación activa en la organización de reuniones tanto nacionales como sectoriales de la sección de refractarios. Durante 40 años, representó a nuestro país, en su calidad de Presidente de ANFRE, ante la Federación Europea de Fabricantes de Productos Refractarios (P.R.E.).

José Rivas Sánchez, fue un ejecutivo fiel cumplidor de sus deberes y compromisos en los cargos que ejercía, de extraordianria capacidad de trabajo y entrega, prestó siempre generosa ayuda a las industrias del ramo, en la solución de sus problemas. Hombres como José Rivas Sánchez, deberíamos tener siempre presente como ejemplo y acicate.

Entre otras condecoraciones, estaba en posesión de la Medalla de Oro del Consejo Superior de Cámaras de la Propiedad Urbana y de la Encomienda de la Orden del Mérito Civil.

La Sociedad Española de Cerámica y Vidrio testimonia su más profunda condolencia a su Viuda Doña Laudivina Alvarez Padrón, a sus hijos y familiares por tan irreparable pérdida.

Boletín de la Sociedad Española de Cerámica y Vidrio. Vol. 34 Núm. 2 Marzo-Abril 1995

65

Publicaciones de la Sociedad Española de Cerámica y Vidrio

	Precio sin IVA	
	Socio	**No socio**
I Semana de estudios cerámicos (Madrid, 1961)	2.000	2.500
II Semana de estudios cerámicos (Madrid, 1963)	2.000	2.500
III Semana de estudios cerámicos (Madrid, 1965)	2.000	2.500
IV Semana de estudios cerámicos (Madrid, 1967)	2.000	2.500
XI Congreso Internacional de Cerámica (Madrid, 1968)	6.000	7.000
Terminología de los defectos del vidrio (Madrid, 1973)	2.500	3.000
Horno eléctrico de arco (I Reunión Monográfica de la Sección de Refractarios, Marbella, 1973). AGOTADO	—	—
El caolín en España (Madrid, 1974). E. Galán Huertos y J. Espinosa de los Monteros	2.000	2.500
Refractarios en colada continua (Madrid, 1974)	—	—
Refractarios en la industria petroquímica (III Reunión Monográfica de la Sección de Refractarios, Puerto de la Cruz, 1976)	2.000	2.500
Refractarios para la industria del cemento (Madrid, 1976). AGOTADO	—	—
Refractarios para tratamiento de acero y cucharas de colada, incluyendo sistemas de cierre de cucharas (XX Coloquio Internacional sobre Refractarios, Aquisgrán, 1977) (Edit. E. Criado)	6.500	7.500
Primeras Jornadas Científicas. El color en la cerámica y el vidrio (Sevilla, 1978)	2.000	2.500
Pastas cerámicas (Madrid, 1979). E. Gippini. AGOTADO	—	—
Segundas Jornadas Científicas. Reactividad de sólidos en cerámica y vidrio (Valencia, 1979)	2.500	3.000
Terceras Jornadas Científicas (Barcelona, 1980)	3.000	4.000
Cuartas Jornadas Científicas (Oviedo, 1981)	3.000	4.000
Separación de fases en vidrios. El sistema $Na_2O.B_2O_3.SiO_2$ (Madrid, 1982). J. Ma. Rincón y A. Durán	2.500	3.000
I Congreso Iberoamericano de Cerámica, Vidrio y Refractarios (dos volúmenes) (Torremolinos, 1982) (Madrid, 1983)	4.500	6.000
Quintas Jornadas Científicas (Santiago de Compostela, 1984)	2.500	3.000
Tablas Cerámicas (Instituto de Química Técnica, Universidad de Valencia). AGOTADO	—	—
Vocabulario para la industria de los materiales refractarios (español-francés-inglés-ruso). UNE 61-000 (Madrid, 1985) (Edit. E. Criado)	4.500	6.000
Jornadas sobre materiales refractarios y siderurgia (Arganda del Rey, 1984) (Madrid, 1985) (Edit. E. Criado)	4.500	6.000
Diccionario cerámico científico-práctico (español-inglés-alemán-francés). C. Guillem Monzonis y M.ª C. Guillem Villar (Valencia, 1987)	5.000	6.000
Curso sobre materias primas para cerámica y vidrio (Edit. J. M.ª González Peña, M. A. Delgado Méndez y J. J. García Rodríguez) (Madrid, 1987). AGOTADO	—	—
Processing of Advanced Ceramics (Edit. J. S. Moya y S. de Aza) (Madrid, 1987)	6.000	7.000
Los materiales cerámicos y vítreos en Extremadura (Edit. J. Ma. Rincón) (Mérida, 1988)	2.000	3.000
Glasses and Glass-Ceramics for Nuclear Waste Management (Edit. J. Ma. Rincón) (2.ª Edición) (también en microficha)	4.000	5.000
Materiales refractarios en siderurgia. Revisión bibliográfica. 1980-1987. —Refractory Materials in Iron & Steelmaking a Bibliographic Review (Edit. E. Criado, A. Pastor y R. Sancho)	6.000	7.000
Ciencia y Tecnología de los Materiales Cerámicos y Vítreos. España'89 (Edit. J. Ma. Rincón) (Faenza Editrice y SECV) (Castellón, 1990)	5.000	5.800
Cerámica y Vidrio'91 (Edit. J. Ma. Rincón, F. Capel y A. Caballero) (Palma, 1991)	2.000	3.000
Nuevos productos y tecnologías de esmaltes y pigmentos cerámicos (Edit. J. Ma. Rincón, J. Carda y J. Alarcón) (1991) (Faenza Editrice y SECV)	4.000	5.000

PEDIDOS

Los pedidos pueden dirigirse a:
Sociedad Española de Cerámica y Vidrio
Ctra. de Valencia, Km. 24,300. 28500 Arganda del Rey (Madrid)
Los envíos se realizarán por transporte urgente a portes debidos.

DOCUMENTACION

La Sociedad Española de Cerámica y Vidrio ofrece a sus socios los siguientes servicios de documentación:
fotocopias de artículos; traducciones de artículos; perfiles bibliográficos; revisiones monográficas.